Double scattering in grazing angle Rutherford backscattering spectra

N.P. Barradas[1,2,*]

[1]   Instituto Tecnológico e Nuclear, Apartado 21, E.N. 10, 2685-953 Sacavém, Portugal

[2]   Centro de Física Nuclear da Universidade de Lisboa, Av. Prof. Gama Pinto 2, 1649-003 Lisboa, Portugal

[*]   e-mail: nunoni@itn.mces.pt

Developments in the analytic model for double scattering in Rutherford backscattering spectra are presented. It is shown that, in grazing angle of incidence spectra of thin films, the main contribution to the low energy tails comes from particles that after the first collision have a path nearly parallel to the surface of the sample. Thus collisions with small scattering angle must be included, since they are the only way of achieving such paths. In bulk samples, these trajectories must also be included. Particle loss as the beam enters the sample, as well as angular dependent screening, are taken into account in the model developed. The effect of lateral spread due to multiple scattering is considered, and its influence in the double scattering spectrum is calculated. It is found to be important in the measurement of ultra-thin films in grazing geometry.

1   Introduction

Analysis of Rutherford backscattering (RBS) is often done by comparing the data with theoretical functions generated by a computer code. The accuracy of the simulations depends, on the one hand, on the accuracy of the stopping power and cross-section databases used, and on the other hand, on the extent to which the ion-solid interactions that occur in the sample are correctly modelled. All analysis codes model single scattering, where the ions of the analysing beam undergo one single large angle scattering event before being detected. Effects such as energy straggling, pulse pileup, or channelling, are taken into account by some codes.

The term plural scattering is normally used to describe trajectories where the ion

suffered several (a few) large angle scattering events before being detected. A particular case is double scattering, corresponding to two large angle scattering events. Multiple scattering refers to the succession of very many small angle scattering events that each ion undergoes (see Figure 1). This separation between plural and multiple scattering is to some extent arbitrary, since it depends on the definition of the terms "large angle" and "small angle" scattering. However, the main effects on the experimental spectra are different, and the theoretical treatment of plural and multiple scattering is normally separated. Plural scattering leads to an increase of the yield at low energies, and to a low energy background. Multiple scattering leads mostly to an additional contribution to energy straggling.

This paper is dedicated to the study of double scattering in RBS spectra, with an emphasis on experiments made at grazing angle of incidence or detection. After reviewing previous work, we show that the grazing angle condition has consequences not previously handled in existing analytic models or codes, leading in some cases to one order of magnitude differences in the background calculated. In particular, the sharp distinction between large and small angle scattering must be abandoned, and in the extreme case of grazing angle analysis of ultra-thin films, the effect of lateral spread due to multiple scattering must be explicitly taken into account in the double scattering calculation.

Examples are shown, covering bulk light element samples, bulk heavy element samples, multilayers, and ultra-thin heavy element films deposited on lighter substrates. The double scattering algorithm now developed has been integrated in the analysis code NDF [1,2].

2   Experimental conditions

RBS was performed with a He$^+$ beam detected at a 160° scattering angle in the Cornell geometry. The angle of incidence θ, defined as the angle between the beam and the surface of the sample, varied between 90º (normal incidence) and 6º (grazing incidence). The beam spot is defined by a rectangular Ta slit system, which is 0.6 mm high, and 0.6 mm and 0.2 wide in the near-normal and grazing incidence experiments, respectively. Experiments were conducted at different times: shortly after the slit was installed; after 10 years of usage without cleaning; and after removing a layer of deposited carbon by mechanical polishing.

3   Double scattering model

3.1   Review of previous work

An early theoretical analysis of the energy spectra of backscattered ions concluded that a low energy background could not be explained even when the effects of straggling and multiple scattering were taken into account, and therefore should be due to other experimental effects [3]. The observation that a low energy background seen in the backscattering spectrum of 280 keV $^4He^{++}$ on a 1130 Å Pt film on SiO_2 was possibly due to plural scattering was made already at the 1st International Conference on Ion Beam Analysis [4]. In the same conference, however, it was noted that scattering of the beam on the beam-defining slits could also contribute to the spectrum at low energies [5]. Further investigations showed that this was the case, and that slit scattering strongly depends on the experimental arrangement [6,7]. It has also been claimed by Gurbich [8] that the low energy background cannot be explained by plural, multiple, and slit scattering alone, which would mean that some significant physical phenomenon is still unaccounted for.

An ad hoc procedure to account for double scattering, consisting in multiplying the calculated yield of a thick sample by an energy-dependent correction factor, has been used [9]. This procedure may lead to the successful analysis of complex RBS spectra [10], but can only be used if a reference sample is available, and provides no information on the physics behind this phenomenon.

A similar correction factor, but due to multiple scattering, was calculated theoretically [11,12]. Multiple scattering leads to angular spread, and the correction factor can be calculated by averaging the cross section over the angular distribution of incoming and outgoing ions. However, the resulting correction is too small to explain the experimental results [13]. An extension of these ideas to plural scattering has been developed [13], with some success in explaining the yield of low energy proton and alpha particle scattering off bulk heavy targets. However, the calculations assume that the plural scattering yield is proportional to the single scattering yield, are valid only for normal incidence, and for target atoms with infinite mass. Furthermore, this methodology can not be used to calculate the low energy backgrounds observed experimentally.

Computer calculation of RBS spectra is normally done by dividing the sample in many sublayers assumed homogeneous, and where the stopping power is assumed to be constant. The beam ions are then followed as they cross the sample, lose energy, and undergo scattering events. To calculate the single scattering spectrum, that is, ignoring plural and multiple scattering, one single ion path must be followed for scattering at each sublayer (see [14] for an early description of the method by Ziegler et al.). The double scattering spectrum can be

calculated using the same methods, but many more trajectories (where trajectory is taken to mean both the path of the ion and its energy along the path) must be considered. For each sublayer, one must consider the first scattering event into the entire solid angle. In practice, one must divide the sphere in a finite number of directions, into which the ion can be scattered. The ion will then suffer a second scattering event, into the direction of the detector. One should note that the energy of the ion after the first scattering event depends on the target atom. If Ns sublayers, Nd first scattering directions, and Na different target atoms are considered, the calculation of the single scattering spectrum involves the calculation of Ns × Na trajectories. The calculation of the double scattering spectrum involves the calculation of approximately Ns^p × Nd × Na^2 trajectories, where $1 < p < 2$ takes into account that three linear segments are considered (before first scattering, between scatterings, and after second scattering). Assuming Ns=100, p=1.5, Nd=120 and Na=5, single scattering requires the calculation of 500 trajectories, and double scattering $3×10^6$.

One must also take care when deciding which paths to consider. The Rutherford cross section is not defined for a 0º scattering angle, and has not been experimentally verified for scattering angles smaller than 15º [15], and usually a minimum limiting angle α_{min} is defined, below which the trajectory is considered to be essentially similar to single scattering.

This approach has been followed by Weber and co-workers [16-18]. To reduce the amount of calculations required, they considered only normal incidence, which leads to symmetry properties of the scattering that can be used effectively. Using α_{min}=15º, they calculated the double scattering background in proton, alpha, and ^{12}C RBS spectra of self-supporting thin films, reproducing well the experimentally observed background only for scattering on Au. In all other cases, the observed background was a factor between 1.6 and 3 times higher than the calculated one. The role of slit scattering in their experiment is unclear. Finally, they provided a simple semi-empirical formula to predict the background intensity in proton scattering, between 0.7 E_{out} and 0.9 E_{out}, where E_{out} is the beam energy for scattering at the surface of the films.

Mayer has continued this work, generalising it to any experimental geometry [19-21]. He used 120 solid angle intervals, and a minimum scattering angle imposed as α_{min}=20º. He obtained excellent results for proton and alpha RBS spectra of heavy thin films on lighter substrates, measured at normal incidence and near-normal detection.

A multiple scattering correction similar to that developed by Serotinin and co-workers for single scattering [11,12] can also be made for the double scattering background, and

preliminary results seem to indicate that it may be a significant contribution in some cases [22]. However, a systematic study has not yet been presented.

Computer calculations using an algorithm similar to the one described above can also be made for elastic recoil detection analysis (ERDA). In the general case, however, several different possibilities must be considered: the incident ion can scatter off a target atom before producing the recoil; the incident ion can produce a recoil which then is scattered off another target atom; the incident ion produces a recoil, which is scattered off a second target atom, which recoils and is then detected. Such calculations have been presented for He-ERDA [23]. In this case, the minimum scattering angle was not a model parameter, but it was calculated on the grounds of an analogy between nuclear and electronic energy loss. The shape of the calculated background reproduced well the experiment, but it was one order of magnitude too low. It should be noted that the calculations presented corresponded to a 10º angle of incidence and detection.

A completely different approach is to perform Monte Carlo simulation of RBS spectra [24-27]. In this case, the effects of plural and multiple scattering are automatically included. The individual contributions of single, double, triple, and higher order scattering, can be studied, depending on the cut-off scattering angle considered as "large angle" scattering. Considering 100 keV protons scattered by a 1000 Å gold target [24], it appears that using a cut-off angle of 23º leads to a calculated Monte Carlo single scattering contribution close to that calculated by the analytic method explained above. An important conclusion was that scattering at small angles has a significant influence on the shape of the low energy background, at least for the low proton beam energies considered; in this case, analytic double scattering models where a minimum scattering angle α_{min} around 15º or 20º is imposed, are not appropriate for quantitative work.

Monte Carlo simulations of plural and multiple scattering in heavy ion RBS have also been done [28]. Recently, these calculations have been extended to heavy ion ERDA [29-34].

Monte Carlo simulations of RBS and ERDA spectra not only require a long calculation time (normally orders of magnitude longer than what it takes to collect the experimental data, although faster implementations are being developed [35]), they also require a considerable degree of expertise by the user, who is in most cases also the author of the code. Monte Carlo methods are thus currently still unsuitable for routine data analysis, for which accurate analytical approaches remain the method of choice.

Finally, one should note that the choice of the value of α_{min} has been one of the main difficulties in previous works, with a wide variety of values being used by different authors in

the different approaches mentioned [16-35].

3.2   Double scattering in grazing angle incidence or detection

As described in the previous section, two reasons have been previously invoked not to consider as double scattering paths where one of the scattering events has a scattering angle smaller than a given value, which can be calculated in some way, but is normally imposed as a given value α_{min}, normally around 20º. The first reason is that those paths are normally considered to be very similar to single scattering; indeed, after a small angle scattering event, the ion continues in more or less the same direction as it had before. This is the reason why trajectory B in Figure 1 is not considered in a double scattering calculation.

The second reason is of a practical nature. The Rutherford cross section is an approximation valid for large angle scattering. If one wishes to include small angle scattering, one must describe the interaction between the projectile and the target accurately, for instance using Ziegler et al.'s universal potential [36]. However, this cannot be easily included in the analytic models used. Instead, one uses the Rutherford cross section including a correction due to screening by the electron clouds. One correction normally used in analysis codes is that of L'Ecuyer et al. [37], which depends on the atomic number of the intervening particles, and on the energy of the incident ion. The correction of Andersen et al. [15] includes an extra term giving an angular dependence, which has been experimentally verified down to 15º. An alternative algorithm for the computation, based on screened Coulomb potentials, of classical cross-sections for screened Coulomb collisions has been presented [38]. It lead to results similar to those of Andersen et al., while it requires a heavier calculation burden.

Consider, however, trajectories B and SB in Figure 2, where a grazing angle of incidence experiment is schematically represented. Trajectory SB corresponds to single scattering, while in trajectory B the ion suffers a fairly small angle scattering event before being backscattered. The path length inside the sample before the large angle scattering event is exactly the same for the two trajectories, and the reasoning above would lead us to discard trajectory B as double scattering. However, first of all, the outgoing path of the ion, after the large angle scattering, is very different in the two trajectories. Also, between the two scattering events the ion is travelling along a path which is parallel to the surface of the sample in trajectory B, which means that it remains within the same layer. On the contrary, in trajectory SB the ion continues to penetrate deeper into the sample, possibly crossing a number of different layers, before being backscattered. Thus, at grazing angle of incidence (or

detection) a small angle scattering event can lead to a trajectory which is fundamentally different, and therefore should be taken into account in a double scattering analytic calculation.

On the contrary, trajectories A and SA are very similar, and trajectory A should indeed be considered as single scattering, in spite of the scattering angles in the two scattering events shown being exactly the same as in trajectory B. The reason is that in trajectory A the ion has a very short path between the two scattering events, therefore not distancing very much from the single scattering trajectory. It becomes clear that, in grazing angle experiments, the angle of scattering cannot be the sole criterion to decide whether a given trajectory corresponds to single or double scattering. Alternative criteria, that take into account the actual path of the ion inside the sample must therefore be found.

First of all, all trajectories where both scattering events have scattering angle larger than $\alpha_{min}=20º$ will be considered. This is the same criterion already used by Weber and co-workers (who used $\alpha_{min}=15º$, that leads to similar results) [16] or Mayer [19], and ensures that double scattering at near-normal incidence and detection geometries will be correctly calculated.

For trajectories where one of the scattering events has scattering angle smaller than α_{min}, only those trajectories that differ in length from the corresponding single scattering trajectory more than a given factor p_{cutoff} will be taken to contribute to the double scattering spectrum. In this work, we chose a minimum path length change of 50%, corresponding to $p_{cutoff} =1.5$. Tests with many different spectra, calculated for different types of samples (including thin and bulk layers, light and heavy elements, and combinations thereof), show that values of p_{cutoff} between around 1.25 and 2 lead to similar results. Smaller values lead to the inclusion of events that are too similar to single scattering, while larger values exclude bona fide double scattering events.

Finally, in order to avoid the singularity at 0º scattering, we exclude all scattering events with angle smaller than 2º. These will only be important in geometries where the angle of incidence or detection is around 2º, which is not normally done in RBS due to problems related to alignment of the beam with the sample, beam spot size, and sample surface flatness.

Another consideration is the number of directions of the first scattering to consider. SIMNRA uses 120 [19], which is normally enough for near-normal incidence and detection geometries. However, in grazing geometries, where the beam can be in a path parallel to the sample surface after the first scattering event, a very small change in scattering angle can lead to large changes in the path, and a much higher density of trajectories must be considered.

Depending on how grazing the geometry is, the algorithm developed divides the 4π sphere into between 500 and 5000 solid angle intervals. These are not all of equal dimension in the algorithm developed, that imposes a much higher density around trajectories nearly parallel to the surface. The selection of trajectories will also depend on the thickness of the layer where the first scattering event takes place, the important point being to ensure that enough different trajectories are calculated where the ion can lose a large fraction of its energy within the layer under consideration (and still have energy enough to be detected afterwards). In this way, the trajectories considered are different in each calculation, and depend both on the experimental geometry and on the sample structure.

3.3   Corrections due to screening and beam particle loss

We thus consider scattering events with scattering angle between 2º and 15º, that is, scattering angles for which experimental confirmation of the Rutherford cross section in the energy range normally used in RBS is not available. However, the screening correction derived by Andersen and co-workers [15] is calculated, with approximations, from the universal interatomic potential, and it agrees well with existing data. Also, double scattering is normally a correction only to the single scattering spectrum. The Andersen et al. angular dependent screening correction is used in the algorithm developed, with the L'Ecuyer et al. correction [37] or no correction at all available as options. In any case, it is clear that any inaccuracy in the scattering cross section used will be reflected in the double scattering spectrum calculated for grazing angle of incidence geometries. Ultimately, the use of a given scattering cross section is to some degree arbitrary, and must be justified by how well experimental results are reproduced.

The strong decrease of the cross section for scattering angles close to zero due to the Andersen et al. screening correction is responsible for the very weak sensitivity of the results to the exact value of p_{cutoff} chosen, for small values of p_{cutoff}. Small values of p_{cutoff} lead to the inclusion of trajectories with low scattering angle, for which the screening correction is very strong.

As the beam travels deeper into the sample, we calculate for each internal sublayer the total scattering cross-section, integrated over the solid angle of all trajectories considered. This leads to particles that are lost from the incoming beam, thus reducing the incoming flux in deeper layers [16]. This effect is not negligible in some cases, for instance at large depths in samples containing heavy elements. This is taken into account in the algorithm developed.

Finally, we note that the scattering cross section corresponding to one given trajectory is not calculated for the actual scattering angle considered, but is integrated over the entire solid angle represented by that trajectory. This is essential at small angles, where the scattering cross section is a rapidly varying function.

3.4   *Influence of lateral spread induced by multiple scattering*

In grazing angle experiments, trajectories where the beam particle has a trajectory which is nearly parallel to the surface account for most of the double scattering spectrum. Consider Figure 3, that represents schematically a grazing angle measurement of an ultra-thin shallow gold layer in a carbon substrate. In trajectory A, the ion is, directly after the first scattering event, in a trajectory parallel to the surface, then travels in a straight line inside the gold layer, and finally is backscattered towards the detector. In reality, multiple scattering inside the gold layer will lead to a succession of small angle deflections, that will be different for each beam particle, leading to a certain lateral spread of the beam after the first scattering event. This will mean that part of the beam that initially is travelling inside the gold layer, will leave this layer and will go to the carbon substrate, as depicted in trajectory B, thus decreasing the particle flux inside the gold layer and increasing it in the carbon layers close to the gold. However, the cross section for a second scattering event off a carbon atom is very small, and most of the beam particles that leave the gold layer due to this process, that would otherwise be detected, will not contribute to the double scattering spectrum.

On the other hand, it is also possible that an ion which suffers a first scattering event off a carbon atom very close to the gold layer, and which is initially in a trajectory nearly parallel to the surface, will enter the gold layer due to lateral spread induced by multiple scattering, as depicted in trajectory C, thus increasing the beam particle flux inside the gold layer. All in all, as the scattering cross section is much higher in heavy elements, both for large and small angle scattering, the net particle flux that travels parallel to the surface in the gold layer will be reduced, leading to a smaller double scattering spectrum.

Therefore, to calculate the double scattering of ultra-thin films measured in grazing angle conditions, one must explicitly take into account the lateral spread due to multiple scattering. We have used the results of Amsel and co-workers [39] to calculate the lateral spread of the beam particles and the resulting changes in the particle flux within each layer. We used the equivalent atomic number approximation for multielemental targets, and also the large energy loss approximation for thick targets. A more accurate treatment has been

proposed by Szilágyi and co-workers and is implemented in the code DEPTH [40]. However, in the context of double scattering the effect of lateral spread is a correction to a correction, and the lower accuracy of the approximations used here is compensated by the increase in calculation speed. One must note that this lateral spread correction can only be important in ultra-thin films, and leads to an increase in calculation time, even with the approximations introduced, of about one order of magnitude, and is therefore a user option in the algorithm developed.

In Figure 4 we show the influence of lateral spread in a C 100 nm / Au 5 nm ($29{\times}10^{15}$ at./cm^2) / C 10 nm ($114{\times}10^{15}$ at./cm^2) trilayer, for a 160° scattering angle and 10° grazing angle of incidence in the Cornell geometry, for 2 MeV ^{4}He. The Au layer was divided internally in three sublayers. It is clear that, inside the Au layer, the beam particle flux after the first scattering event rapidly decreases with lateral depth (that is, with the length of the path traversed by the ions in a direction parallel to the surface). The decrease is stronger in the lateral sublayers, corresponding to the edges of the Au layer; while the centre of the Au layer receives beam particles lost from the edge Au layers, these receive very little from the adjacent C. The effect is however small, and the double scattering spectrum calculated dividing the Au layer in three internal layers or treating it as a single internal layer (not shown), is practically the same. On the other hand, it is essential to consider both the particles lost to and gained from adjacent layers.

The corresponding calculated energy spectra are shown in Figure 5. The oscillations or steps seen around channels 320 and 400 are an artefact due to the limited number of trajectories used in the calculation (around 2000), in this very difficult case; using a larger number of trajectories (around 5000) transforms these steps in a smooth curve. It is clear that using a hard cut-off angle α_{min}=20° leads to a double scattering spectrum of a similar shape, but one order of magnitude smaller as compared to the algorithm now developed. On the other hand, the influence of lateral spread, even in this example designed to maximise it, is at most a factor of two at low energies.

Finally, one should note that, for each internal layer, the effect of lateral spread is considered to be symmetrical, which is not strictly true. The same approximation is used in the multiple scattering theory that leads to the lateral spread calculations [39].

3.5   *Algorithmic issues*

The scattering cross section has a strong angular dependence. In order to reduce the calculation time, we calculate only the trajectories with a higher cross-section, corresponding

to a total of 99% of the integrated cross section of all trajectories initially considered. In other words, we reject trajectories corresponding to 1% of the total cross section. The resulting calculated double scattering spectra are numerically different, but the difference is hardly seen on a plot. In grazing angle of incidence, where most of the cross section is concentrated in trajectories with small scattering angles, this can correspond to 50% to 90% of all trajectories, leading to an up to one order of magnitude efficiency gain.

Furthermore, the scattering cross section is proportional to the square of the atomic number of the target element. This means that a trajectory that involves two scattering events off light elements is very unlikely. In the algorithm developed, we take into account the concentration of the elements present in the sample, to approximately calculate the total cross section for all the different double scattering possibilities of first scatterer/second scatterer pairs. We then reject pairs corresponding to 1% of the total cross section. Again, the effect on the calculated double scattering spectrum is minimal.

Straggling is not calculated for double scattering in the present implementation, since it would lead to an increase of calculation time of over one order of magnitude. The system resolution is however convoluted with the double scattering spectrum.

One must stress that double scattering is not the only effect that may lead to a measured yield different from a single scattering calculation. Other effects are energy straggling, pulse pileup, channelling, inaccurate stopping power values, and even the simple fact that the real sample composition may be different from what is input to the simulation. In particular, the effect of energy straggling on the shape of the low energy part of RBS spectra is often dramatic. For instance, in grazing angle geometries, multiple scattering is the main contribution to the rapid deterioration of the energy resolution, and if it is not taken into account, the shape of the calculated spectrum at low energies can be dramatically different. Furthermore, even when energy loss straggling is taken into account, algorithmic issues may lead to poor simulations: due to the statistical nature of energy loss, a correct simulation must follow particles up to depths greater than the maximum depth at which particles with the average beam energy may be scattered and still emerge from the sample with positive energy. To our knowledge, no analytic codes exist that actually do that, so all of them calculate a distorted single scattering spectrum at low energies. DEPTH implements a partial solution to this problem, which is nevertheless not accurate [41].

4   Results

RBS spectra of a Si/SiO$_2$ 498 nm sample taken at normal incidence and different beam energies, previously measured at CNR-IMM-Sezione di Bologna and published by C. Pascual-Izarra et al. in Ref. [42], are shown in Figure 6. The calculated double scattering contributions are shown as dashed lines. Recently determined accurate stopping powers for Si [43] and SiO$_2$ [42] were used. The cross sections determined by Cheng et al. were used in the E=3 MeV simulation [44] Nearly perfect simulations are obtained, which was expected for a normal incidence experiment. As expected, the double scattering contribution is very small in a sample composed of light elements.

RBS spectra of a GaSb/AlGaSb sample are shown in Figure 7 [45]. Different thin layers with different Al concentration are deposited on top of bulk GaSb. The beam energy was 2 MeV. At non-grazing incidence (θ=50º), the calculated double scattering contribution is entirely due to trajectories where both scattering events have scattering angle larger than α_{min} = 20º. At grazing incidence (θ=8º), however, if the trajectories with one scattering event smaller than 20º are rejected a priori, the calculated spectrum strongly diverges from the data. On the contrary, with the algorithm now developed, the agreement is excellent, except at very low energies, where even a small inaccuracy in the stopping powers used (SRIM2000 [36]) may lead to the difference observed.

RBS spectra of a Si/Re 50 Å/(Co 20Å/Re 5Å)$_{16}$ sample, collected with a 1 MeV beam, are shown in Figure 8. They were collected shortly after the beam-defining slit system was installed, and they have been previously published in ref. [46]. The known layer roughness is included in the simulation using the algorithms described in refs. [47,48]. The depth resolution as a function of depth was calculated with DEPTH [40], which is called automatically within NDF [1,2].

The signal of the 50Å Re buffer layer is not well reproduced in the θ=12º spectrum, indicating the existence of diffusion between the buffer and the Si substrate that was not considered in the simulation. This may be partly responsible for the strong distortion of the signal around channels 75-150 observed for θ between 8º and 6º, but the main reason behind that is probably the inaccuracy due to the straggling calculation, as mentioned at the end of section 3.5 above.

Double scattering is a major contribution at very grazing angles in this sample composed of fairly heavy elements. In spite of the distortion in the calculated spectra, it should be noted that the double scattering calculation reproduces extremely well the yield at

very low energies for all angles of incidence, only when the Andersen et al. screening correction [15] is used. When no correction is applied, or the L'Ecuyer correction is used (which does not take into account the dependence on the scattering angle) [37], the calculated spectrum is much higher than the data. The exception is for $\theta=45°$, where trajectories with small angle scattering do not influence the calculation. Finally, when the $\alpha_{min}=20°$ cut-off is strictly imposed, the calculated double scattering spectrum is close to zero, which is not realistic.

The RBS spectrum of a C/Ta 22Å/CoFe 28Å/Al$_2$O$_3$ 6Å/CoFe 30Å/Ta 26Å/Ta$_2$O$_5$ 23Å/C 27Å sample is shown in Figure 9. The Ta has a 1 at.% Ar contamination. The metal layers also have a 2 at.% Si contamination. The beam energy was 2 MeV and the angle of incidence was 10°. The experiment was conducted 10 years after the beam-defining slit system was installed, without any cleaning being done in that period. First of all, one should note that imposing a $\alpha_{min}=20°$ cut-off limit leads to a double scattering spectrum which has the same shape, but is about one order of magnitude smaller, than the measured spectrum. On the other hand, the background calculated with the algorithm presented in this paper agrees qualitatively well with the measured background.

Quantitatively, agreement is nearly perfect when the effect of lateral spread due to multiple scattering is not included in the calculation. When this effect is included, the background in channels 100-150 is slightly underestimated. This is unexpected, since multiple scattering is a well-known reality and, from a theoretical point of view, it must lead to angular spread and the concomitant loss of beam particle flux in the layers composed of the heavier elements. One possible explanation is enhanced slit scattering, due for instance to accumulated carbon on the slits or to surface roughness in the slits due to accumulated beam-induced damage. This would also explain the misfit below channel 100, although that could also be explained by a slightly inaccurate ^{4}He in C stopping powers or straggling calculation.

We measured the same sample after mechanical polishing the slits. Unfortunately, this was done more than two years after the original experiment, and sample oxidation and degradation does not allow us to take definite conclusions. In order to test the existence of slit scattering, experiments were conducted with different slit widths, from 0.2 to 0.8 mm. The measured background in the region of the oxygen and aluminium signal is respectively 20±6% and 7±5% larger when the slit width is reduced from 0.8 to 0.2 mm.

5   Conclusions

Developments in the analytic model for double scattering in Rutherford backscattering spectra were presented. It is shown that, in grazing angle of incidence spectra of ultra-thin films, the main contribution to the low energy tails comes from particles that after the first collision have a path nearly parallel to the surface of the sample. Thus collisions with small scattering angle must be included, since they are the only way of achieving such paths. In bulk samples, these trajectories must also be included. In some cases, the difference in the background calculated is one order of magnitude.

Particle loss as the beam enters the sample, as well as angular dependent screening, are taken into account in the model developed. The effect of lateral spread due to multiple scattering is also considered, and its influence in the double scattering spectrum is calculated. It is found to be important in the measurement of ultra-thin films in grazing geometry.

Examples are shown, covering bulk light element samples, bulk heavy element samples, multilayers, and ultra-thin heavy element films deposited on lighter substrates. Good quantitative agreement between calculations and experiments is found for near-normal and grazing angle experimental geometries, both in the reproduction of the enhancement of the signal in bulk samples, and in the low energy background observed in thin film samples. Further contributions to the signal coming, for instance, from slit scattering, cannot however be ruled out.

The double scattering algorithm now developed has been integrated in the analysis code NDF [1,2].

Acknowledgments

References

[1]   N. P. Barradas, C. Jeynes, R. P. Webb, Appl. Phys. Lett. 71 (1997) 291.

[2]   C. Jeynes, N.P. Barradas, P.K. Marriott, M. Jenkin, E. Wendler, G. Boudreault, R.P. Webb, J. Phys. D: Appl. Phys. 36 (2003) R97. http://www.ee.surrey.ac.uk/ibc/ndf/

[3]   D. K. Brice, Thin Solid Films, 19 (1973) 121.

[4]   B. M. U. Scherzer, P. Børgesen, M.-A. Nicolet, J. W. Mayer, in: Ion Beam Surface Layer Analysis ed. O. Meyer, G. Linker, F. Käppeler (Plenum Press, New York, 1976).

[5]   R. S. Blewer, in: Ion Beam Surface Layer Analysis ed. O. Meyer, G. Linker, F. Käppeler (Plenum Press, New York, 1976).

[6]   L. Varga, Nucl. Instrum. Methods B17 (1986) 260.

[7]   S. I. Bazhukov, A. V. Kibardin, T. M. Pyatkova, Nucl. Instrum. Methods B58 (1991) 242.

[8]   A. F. Gurbich, Nucl. Instrum. Methods A364 (1995) 496.

[9]   J. A. Moore, Nucl. Instrum. Methods 174 (1980) 577.

[10]   N. P. Barradas, C. Jeynes, S. M. Jackson, Nucl. Instrum. Methods B136-138 (1998) 1168.

[11]   V. Ya. Chumanov, Sh. Z. Izmailov, G. P. Pokhil, E. I. Sirotinin, A. F. Tulinov, Phys. Status Solidi A53 (1979) 51.

[12]   E. I. Sirotinin, A. F. Tulinov, V. A. Khodyrev, V. N. Mizgulin, Nucl. Instrum. Methods B4 (1984) 337.

[13]   Ž. Šmit, Phys. Rev. A48 (1993) 2070.

[14]   J. F. Ziegler, R. F. Lever, J. K. Hirvonen, in: Ion Beam Surface Layer Analysis ed. O. Meyer, G. Linker, F. Käppeler (Plenum Press, New York, 1976).

[15]   H. H. Andersen, F. Besenbacher, P. Loftager, W. Möller, Phys. Rev. A21 (1980) 1891.

[16]   A. Weber, H. Mommsen, W. Sarter, A. Weller, Nucl. Instrum. Methods 198 (1982) 527.

[17]   A. Weber, H. Mommsen, Nucl. Instrum. Methods 204 (1983) 559.

[18]   A. Weber, Q. Fazly, H. Mommsen, Nucl. Instrum. Methods B4 (1984) 79.

[19]   M. Mayer, *SIMNRA User's Guide*, Report IPP 9/113, Max-Planck-Institut für Plasmaphysik, Garching, Germany, 1997.

[20]   W. Eckstein, M. Mayer, Nucl. Instrum. Methods B153 (1999) 337.

[21]   M. Mayer, Nucl. Instrum. Methods B194 (2002) 177.

[22]   J. P. Stoquert, private communication.

[23] F. Repplinger, J. P. Stoquert, P. Siffert, Nucl. Intrum. Methods B80/81 (1993) 24.

[24] E. Steinbauer, P. Bauer, J. Biersack, Nucl. Instrum. Methods B45 (1990) 171.

[25] J. Biersack, E. Steinbauer, P. Bauer, Nucl. Instrum. Methods B61 (1991) 77.

[26] P. Bauer, E. Steinbauer, J. Biersack, Nucl. Instrum. Methods B64 (1992) 711.

[27] E. Steinbauer, P. Bauer, J. Biersack, G. Bortels, Rad. Eff. Def. Solids 130-131 (1994) 77.

[28] M. M. Li, D. J. O'Connor, Nucl. Instrum. Methods B149 (1999) 460.

[29] P. N. Johnston, R. D. Franich, I. F. Bubb, M. El Bouanani, D. D. Cohen, N. Dytlewski, R. Siegele, Nucl. Instrum. Methods B161-163 (2000) 314.

[30] K. Arstila, T. Sajavaara, J. Keinonen, Nucl. Instrum. Methods B174 (2001) 163.

[31] R. D. Franich, P. N. Johnston, I. F. Bubb, N. Dytlewski, D. D. Cohen, Nucl. Instrum. Methods B190 (2002) 252.

[32] R. D. Franich, P. N. Johnston, I. F. Bubb, AIP Conference Proceedings 680 (2003) 385.

[33] K. Arstila , J. A. Knapp , K. Nordlund, B. L. Doyle, Nucl. Instrum. Methods B (2004), accepted (Proc. IBA16).

[34] R. D. Franich , P. N. Johnston, I. F. Bubb, Nucl. Instrum. Methods B (2004), accepted (Proc. IBA16).

[35] P. Pusa, T. Ahlgren, E. Rauhala, Nucl. Instrum. Methods B (2004), accepted (Proc. IBA16).

[36] J. F. Ziegler, J. P. Biersack, U. Littmark, The Stopping and Range of Ions in Solids (Pergamon, New York, 1985).

[37] J. L'Ecuyer, J. A. Davies, N. Matsunami, Nucl. Instrum. Methods 160 (1979) 337.

[38] M. H. Mendenhall, R. A. Weller, Nucl. Instrum. Methods B58 (1991) 11.

[39] G. Amsel, G. Battistig, A. L'Hoir, Nucl. Instrum. Methods B201 (2003) 325.

[40] E. Szilágyi, F. Pászti, G. Amsel, Nucl. Instrum. Methods B100 (1995) 103. DEPTH can be downloaded free of charge from http://www.kfki.hu/~ionhp/

[41] E. Szilágyi, Nucl. Instrum. Methods B161 (2000) 37.

[42] C. Pascual-Izarra, M. Bianconi, G. Lulli, C. Summonte, Nucl. Instrum. Methods B196 (2002) 209.

[43] N. P. Barradas, C. Jeynes, R. P. Webb, E. Wendler, Nucl. Instrum. Methods B194 (2002) 15.

[44] H. S. Cheng, H. Shen, J. Y. Tang, F. Yang , Nucl. Instrum. Methods B83 (1993) 449.

[45] N. P. Barradas, C. M. Ruiz, E. Alves, E. Diéguez, F. Dimroth, M.-A. Chenot, A. Bett,

Nucl. Instrum. Methods B (2004) (in press).

[46] N. P. Barradas, J. C. Soares, M. F. da Silva, F. Pászti, E. Szilágyi, Nucl. Instrum. Methods B94 (1994) 266.

[47] N. P. Barradas, J. Phys. D: Appl. Phys. 34 (2001) 2109

[48] N. P. Barradas, E Alves, S. Pereira, V. V. Shvartsman, A. L. Kholkin, E. Pereira, K. P. O'Donnell, C. Liu, C. J. Deatcher I. M. Watson, M. Mayer, Nucl. Instrum. Methods B 217 (2004) 479.

Figure Captions

Figure 1. Schematic representation of ion scattering. Trajectories A and C correspond to single and double scattering, respectively. Trajectories B and D correspond to multiple scattering (including one large angle single scattering event).

Figure 2. Schematic representation of ion scattering at grazing angle of incidence.

Figure 3. Schematic representation of the interaction between multiple and double scattering at grazing angle of incidence.

Figure 4. Influence of lateral spread in a C 100 nm / Au 5 nm ($29{\times}10^{15}$ at./cm^2) / C 10 nm ($114{\times}10^{15}$ at./cm^2) trilayer, for a 160º scattering angle and 10º grazing angle of incidence in the Cornell geometry, for 2 MeV ^{4}He. The Au layer was divided internally in three sublayers. a) Flux of particles that travel in a direction parallel to the sample surface after being scattered at a given depth, normalised at lateral depth zero. b) Flux in the centre and edge gold sublayers, normalised at lateral depth zero. The flux that one would obtain at the centre of the Au layer if one would consider only the beam particles lost to, and not those gained from, the edges of the Au layer, is also shown.

Figure 5. Energy spectra calculated for a C 100 nm / Au 5 nm / C 10 nm trilayer (solid lines), for a 160º scattering angle and 10º grazing angle of incidence in the Cornell geometry, for 2 MeV ^{4}He. The double scattering contributions are shown: considering only scattering events with $\alpha_{min} \geq 20º$ (dashed-dotted line); and with the full algorithm with (dotted line) and without (dashed line) the lateral spread effect.

Figure 6. Normal incidence RBS spectra of a Si/SiO$_2$ 498 nm sample taken at different beam energies. The calculated double scattering contributions are shown as dashed lines.

Figure 7. 2 MeV ^{4}He RBS spectra of a GaSb/AlGaSb sample. Upper and lower solid lines: simulation with and without the double scattering contribution. Dashed-dotted

lines: partial single scattering spectra of Ga and Sb. Dasehd line: double scattering spectrum with Andersen et al. screening. For θ=8º, the upper dotted line is the double scattering spectrum with L'Ecuyer et al. screening, and the lower dotted line is the double scattering spectrum imposing a strict α_{min}=20º cutoff angle.

Figure 8. 1 MeV ^{4}He RBS spectra of a Si/Re 50 Å/(Co 20Å/Re 5Å)$_{16}$ sample. Solid line: simulation. Dashed line: double scattering spectrum with Andersen et al. screening. Upper dotted line and dashed-dotted line: double scattering spectrum with no screening and with L'Ecuyer et al. screening, respectively. Lower dotted line: double scattering spectrum imposing a strict α_{min}=20º cutoff angle.

Figure 9. RBS spectrum of a C/Ta 22Å/CoFe 28Å/Al$_2$O$_3$ 6Å/CoFe 30Å/Ta 26Å/Ta$_2$O$_5$ 23Å/C 27Å sample, for 2 MeV ^{4}He and 10º grazing angle of incidence. a) Solid line: simulation including double scattering. Dashed line: single scattering contribution. Dotted line: double scattering contribution without lateral spread effect. Dashed-dotted line: double scattering spectrum imposing a strict α_{min}=20º cutoff angle. b) Solid line: simulation including double scattering. Dotted and dashed line: double scattering contribution with and without lateral spread effect, respectively.
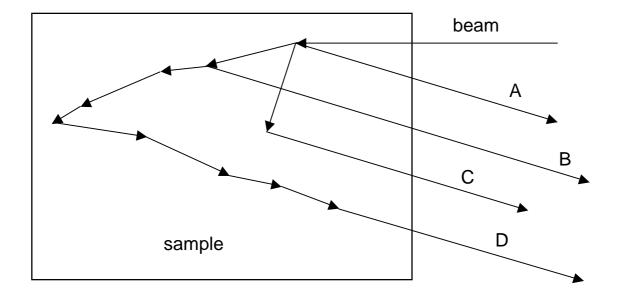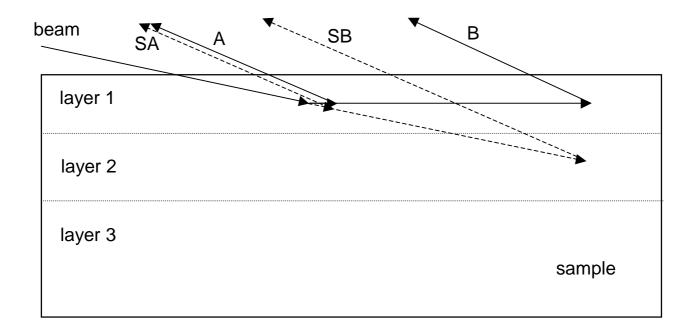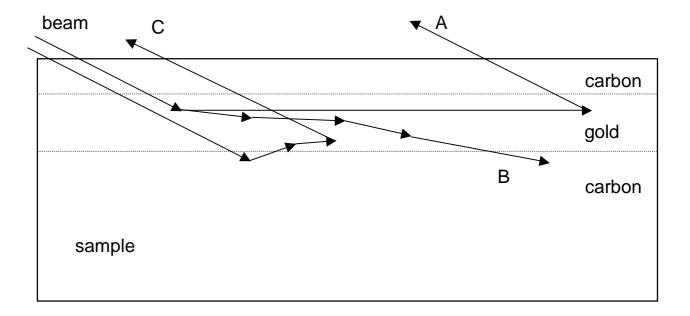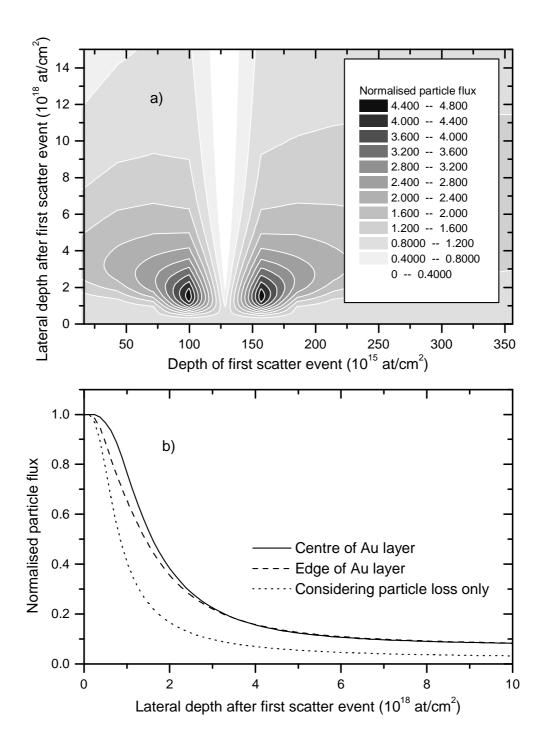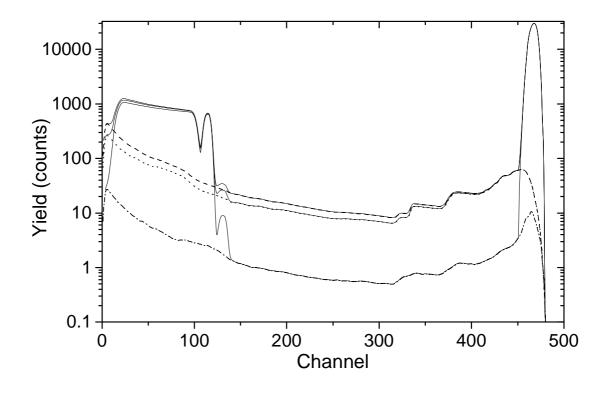
Fig. 1

Fig. 2

Fig. 3

Fig. 4

Fig. 5

Fig. 6

Fig. 7

Fig. 8

Fig. 9